SMRT repression of nuclear receptors controls the adipogenic set point and metabolic homeostasis

Russell R. Nofsinger[a], Pingping Li[b], Suk-Hyun Hong[a], Johan W. Jonker[a], Grant D. Barish[a], Hao Ying[c], Sheue-yann Cheng[c], Mathias LeBlanc[a], Wei Xu[d], Liming Pei[a], Yeon-Joo Kang[e], Michael Nelson[a], Michael Downes[a], Ruth T. Yu[a], Jerrold M. Olefsky[b], Chih-Hao Lee[f], and Ronald M. Evans[a,g,1]

[a]Gene Expression Laboratory, Salk Institute for Biological Studies, 10010 North Torrey Pines Road, La Jolla, CA 92037; [b]Department of Medicine, University of California at San Diego, 9500 Gilman Drive, MC0673, La Jolla, CA 92093; [c]Laboratory of Molecular Biology, Center for Cancer Research, National Cancer Institute, National Institutes of Health, Bethesda, MD 20892; [d]McArdle Laboratory for Cancer Research, University of Wisconsin, 1400 University Avenue, Madison, WI 53706; [e]Center for Neuroscience, Aging, and Stem Cell Research, Burnham Institute for Medical Research, 10901 North Torrey Pines Road, La Jolla, CA 92037; [f]Department of Genetics and Complex Diseases, Harvard School of Public Health, 665 Huntington Avenue, Boston, MA 02115; and [g]Howard Hughes Medical Institute, Salk Institute for Biological Studies, 10010 North Torrey Pines Road, La Jolla, CA 92037

Contributed by Ronald M. Evans, October 30, 2008 (sent for review October 7, 2008)

The nuclear receptor corepressor, silencing mediator of retinoid and thyroid hormone receptors (SMRT), is recruited by a plethora of transcription factors to mediate lineage and signal-dependent transcriptional repression. We generated a knockin mutation in the receptor interaction domain (RID) of SMRT (SMRT^{mRID}) that solely disrupts its interaction with nuclear hormone receptors (NHRs). SMRT^{mRID} mice are viable and exhibit no gross developmental abnormalities, demonstrating that the reported lethality of SMRT knockouts is determined by non-NHR transcription factors. However, SMRT^{mRID} mice exhibit widespread metabolic defects including reduced respiration, altered insulin sensitivity, and 70% increased adiposity. The latter phenotype is illustrated by the observation that SMRT^{mRID}-derived MEFs display a dramatically increased adipogenic capacity and accelerated differentiation rate. Collectively, our results demonstrate that SMRT-RID-dependent repression is a key determinant of the adipogenic set point as well as an integrator of glucose metabolism and whole-body metabolic homeostasis.

adipogenesis | corepressor | PPAR | TR | glucose regulation

The nuclear hormone receptor (NHR) superfamily comprises 48 transcription factors that serve as pleiotropic regulators of a wide variety of biological processes. In the standard model of NHR action, ligand binding is believed to actuate a bifunctional molecular switch, releasing the repressive corepressor complex and recruiting a histone acetyltransferase coactivator complex, resulting in potent transcriptional activation of gene targets (1). Investigation of NHR agonists and genetic models of NHR coactivators have revealed critical roles for NHR-dependent transcriptional activation in metabolic homeostasis and development (2–7); however, the impact of NHR-mediated gene repression through their associated corepressors is less defined. Although SMRT and nuclear receptor corepressor (NCoR) are prototypical NHR corepressors, they also associate with >10 distinct classes of transcription factors including MyoD, p53, Myc, Foxo1, and Ptx1 (8). Therefore, it is not surprising that whole-body gene knockouts (KOs) of either corepressor result in embryonic lethality. Genetic deletion of NCoR results in defects in CNS, erythrocyte, and thymocyte development, whereas SMRT deletion causes brain and heart pathology (9, 10). However, the extent to which NHRs are involved in these phenotypes remains unclear.

Five amino acids referred to as the CoRNR box motif delineate the NHR interaction surface within each of the receptor-interacting domains (RIDs) of the corepressors (11). The precise mapping and characterization of the SMRT RIDs suggested a unique strategy to selectively inhibit SMRT's corepressor activities in the context of NHRs (12, 13). To this end, we generated knockin mice (SMRT^{mRID}) harboring point mutations within the SMRT CoRNR boxes (RIDs 1 and 2) to specifically disrupt the interaction between SMRT and NHRs (S.-H.H., R.R.N., R.M.E., unpublished work). The specific disruption of the SMRT–NHR interaction resulted in viable mice that displayed normal organogenesis. This demonstrates that the lethality of SMRT knockout mice depends on non-NHR transcription factors. However, SMRT^{mRID} mice develop a multitude of metabolic derangements that include increased adiposity, depressed metabolic rate, and insulin resistance demonstrating that SMRT-RID-dependent repression is a key determinant of the adipogenic set point as well as an integrator of whole-body metabolic homeostasis.

Results

Generation and Validation of SMRT^{mRID} Knockin Mice. To study the in vivo role of SMRT-mediated NHR repression, we generated knockin mice (SMRT^{mRID}) harboring alanine mutations in the SMRT-RID1 and 2 domains (Fig. 1*A*). Two-hybrid analysis confirmed that these specific mutations severely disrupted interaction with NHRs, including RAR, TR, and PPAR subfamilies (Fig. 1*B*). Homozygous SMRT^{mRID} mice were viable and expressed levels of endogenous SMRT and NCoR mRNA and protein in tissues and primary cells comparable to wild-type (wt) animals, suggesting that the RID mutations did not result in compensatory changes in corepressor expression (supporting information (SI) Fig. S1 and data not shown). Although SMRT^{mRID} mice exhibit no gross morphological defects, mutant mice are ≈10% lighter than wt littermates (Fig. 1*C*). Histological evaluation of SMRT^{mRID} mice revealed normal heart and brain development (Fig. 1 *D* and *E* and data not shown), contrasting with the defects reported in SMRT$^{-/-}$ animals. The corpus callosum, anterior commissure, and hippocampal commissure in SMRT^{mRID} brains were of comparable size and morphology to wt controls (Fig. 1*D*). Although a slightly thinner ventricular wall was noted in the SMRT^{mRID} hearts at birth, this abnormality subsided by adulthood (Fig. 1*E*). Together, these findings show that SMRT–NHR signaling is not required during development and suggest that the reported embryonic lethality of SMRT knockout mice is mediated by non-NHR transcription factors.

Author contributions: R.R.N., C.-H.L., and R.M.E. designed research; R.R.N., P.L., S.-H.H., J.W.J., H.Y., S.-y.C., W.X., L.P., Y.-J.K., and M.N. performed research; R.R.N. and J.W.J. contributed new reagents/analytic tools; R.R.N., P.L., S.-H.H., J.W.J., G.D.B., M.L., M.D., R.T.Y., J.M.O., C.-H.L., and R.M.E. analyzed data; and R.R.N., J.W.J., G.D.B., M.D., R.T.Y., and R.M.E. wrote the paper.

The authors declare no conflict of interest.

Freely available online through the PNAS open access option.

Data deposition: The GeneChip analysis data reported in this paper have been deposited in the Gene Expression Omnibus (GEO) database, www.ncbi.nlm.nih.gov/geo (accession no. GSE13143).

[1]To whom correspondence should be addressed. E-mail: evans@salk.edu.

This article contains supporting information online at www.pnas.org/cgi/content/full/0811012105/DCSupplemental.

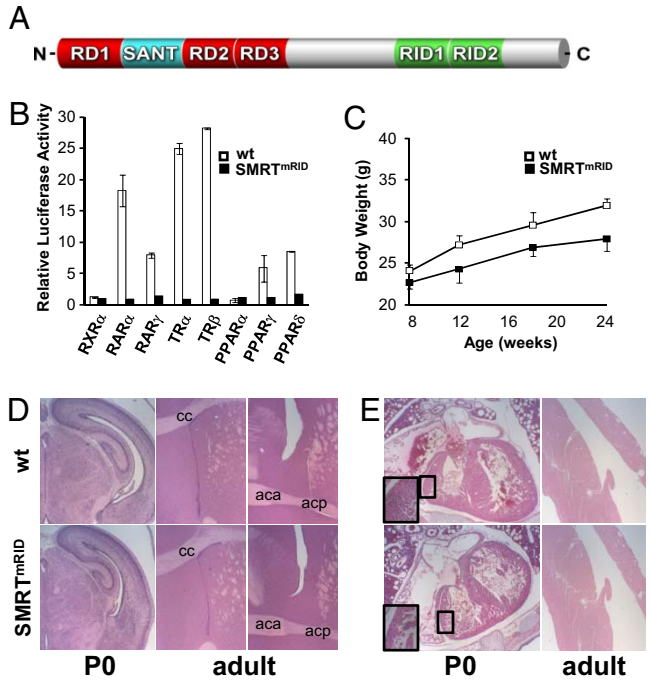

Fig. 1. Characterization of SMRT^{mRID} mice. (*A*) Schematic of SMRT functional domains. (*B*) Mammalian 2-hybrid experiment showing interaction of wt and SMRT^{mRID} Gal4-SMRT and indicated VP16-NHR-LBD fusion proteins in CV-1 cells. (*C*) Reduced body weights in SMRT^{mRID} mice compared with wt littermates are observed from 8 to 24 weeks of age. (*D*) H&E-stained sections of SMRT^{mRID} brains in P0 and adult mice reveal no apparent defects. Corpus callosum (cc) and anterior commissure (aca, acp) are indicated. (*E*) H&E-stained sections of SMRT^{mRID} heart reveal a thinner ventricular wall (boxed area shown magnified in lower left corner) at P0 compared with wt. By 4 months of age, SMRT^{mRID} hearts exhibit normal ventricular wall thickness.

Metabolic Parameters of SMRT^{mRID} Mice. At 10 weeks of age, SMRT^{mRID} mice have decreased metabolic rates (presented as heat) and expend nearly 20% less energy than controls (Fig. 2*A*). Additionally, respiratory rates were decreased in mutant mice in both active and resting states. As a result of the relatively larger reduction in VCO_2, the respiratory exchange ratio (RER = VCO_2/VO_2) was significantly reduced (Fig. 2*A*), indicating that an increased proportion of fuel utilization in these mice is met through fatty acid oxidation.

Thyroid Hormone Signaling Dysregulation in SMRT^{mRID} Mice. Thyroid hormone broadly impacts whole-body metabolism, controlling oxygen consumption in virtually every tissue. These effects are largely mediated through thyroid hormone α or β receptors (TRs) that activate or, alternatively, repress gene expression on binding to ligand. The anticipated disruption of SMRT–TR interactions conferred by the RID mutations (Fig. 1*A*) and decreased energy utilization in SMRT mutant animals (Fig. 2*A*) suggested possible dysregulation of TR signaling in SMRT^{mRID} mice. The liver is a key metabolic organ through which thyroid hormone influences lipid and glucose metabolism. TRs control the expression of hepatic genes involved both in cholesterol uptake (Ldlr and Srb-1) and synthesis (HMG-CoA reductase), and a net effect of TR activation is the lowering of circulating cholesterol levels. Under normal conditions, serum cholesterol levels were similar among wt and SMRT^{mRID} mice, but when rendered hypothyroid with propylthiouracil/methimazole (PTU/MMI) treatment, the resulting hypercholesterolemia was significantly attenuated in SMRT^{mRID} mice (Fig. 2*B*). Consistent with these results, expression of Ldlr, Sr-b1, and HMG-CoA reductase was significantly higher in PTU/MMI-treated SMRT^{mRID} livers (Fig. 2*C*). De-repression of additional TR target genes in the liver was also observed, including the lipogenic genes, fatty acid synthase (FAS), and malic enzyme (ME). Spot14 and Cyp7a1, other TR targets, were up-regulated, albeit not to significant levels (Fig. S2). Srebp-1c, a regulator of Spot14 and FAS, but not a TR target gene, was unchanged (Fig. S2). Interestingly, the negatively regulated pituitary TR target genes TSHα and TSHβ, as well as serum TSH levels are not up-regulated in SMRT^{mRID} mice at baseline or with PTU/MMI treatment, indicating that SMRT association with TR is not required for ligand-induced negative regulation (Fig. 2 *D* and *E*). Conversely, these results do demonstrate that SMRT controls positively regulated TR target genes in vivo and that hypothyroidism is a SMRT-dependent phenomenon.

Aberrant Glucose Homeostasis in SMRT^{mRID} Mice. The altered substrate utilization and perturbed TR signaling observed in SMRT^{mRID} mice raised questions about the impact of SMRT de-repression on glucose homeostasis. For example, hyperthyroidism is known to increase hepatic glucose output. Indeed, fasting blood glucose levels were significantly higher in SMRT^{mRID} mice compared with littermate controls (Figs. 2 *F* and *G*). Intraperitoneal challenge of mice with 1.5 mg/g glucose demonstrated glucose intolerance in SMRT^{mRID} mice, which had significantly higher excursions throughout a 120-min period after the injection (Fig. 2*F*). To gain insight into the aberrant control of blood glucose in SMRT^{mRID} animals, we performed hyperinsulinemic-euglycemic clamping on chow-fed, weight-matched littermates. SMRT^{mRID} animals displayed higher baseline hepatic glucose production (HGP), but their HGP was suppressed normally after insulin injection (Fig. 2*G Left Center*). Moreover, the significantly diminished insulin-stimulated increase in glucose disposal rate in SMRT^{mRID} mice (Fig. 2*G Right Center*), suggests an insulin-resistant muscle, a feature also common in hyperthyroidism.

Unexpectedly, SMRT^{mRID} mice had fasting and insulin-suppressed free fatty acid levels comparable with wt controls (Fig. 2*G Right*), indicating that their adipose tissue displays normal insulin sensitivity. Consistent with this observation, the epididymal fat pad (EFP) to body weight (BW) ratio was nearly 70% increased in SMRT^{mRID} mice compared with wt controls. Furthermore, chemical body composition analysis demonstrated an increase in overall body lipid content (Fig. 2*H*). Analysis of mice fed a high-fat, high-carbohydrate diet (HFD) revealed similar proportional increases in EFP/BW ratios and overall lipid composition (data not shown). Histological examination of fat pads from SMRT^{mRID} mice revealed white adipocytes of a size comparable to controls (Fig. S3), suggesting that the increased fat mass is the result of increased adipogenesis rather than lipid accumulation in existing adipocytes. Adiponectin, an adipose-tissue-derived endocrine hormone that is strongly correlated with insulin sensitivity is significantly higher in SMRT^{mRID} animals (Fig. 2*I*). This suggests that the locally generated insulin sensitivity of the adipose tissue is insufficient to overcome the more global context of glucose intolerance, insulin resistance, and adiposity in these mice.

SMRT^{mRID} Cells Have a Proadipogenic Profile. The predisposition of SMRT^{mRID} mice to increased adiposity led us to explore the adipogenic properties of SMRT^{mRID}- and wt-derived transformed MEF lines. Consistent with previous observations, differentiation cocktail [DC; 1 μM dexamethasone (DEX), 5 μg/ml insulin, 0.5 mM isobutylmethylxanthine (IBMX), 1 μM Rosiglitazone (Rosi)] induces ≈5% of wt cells to become mature adipocytes as indicated by accumulation of Oil Red O. Despite the success and utility of this assay, little is known as to how 95% of cells are refractory to this trigger. Surprisingly, we observed a nearly 100% differentiation of SMRT^{mRID}-derived MEFs suggesting that MEFs have an adipogenic potential that is restricted by active SMRT-dependent NHR repression (Fig. 3*A*). Similar heightened differentiation potentials were observed in multiple independently

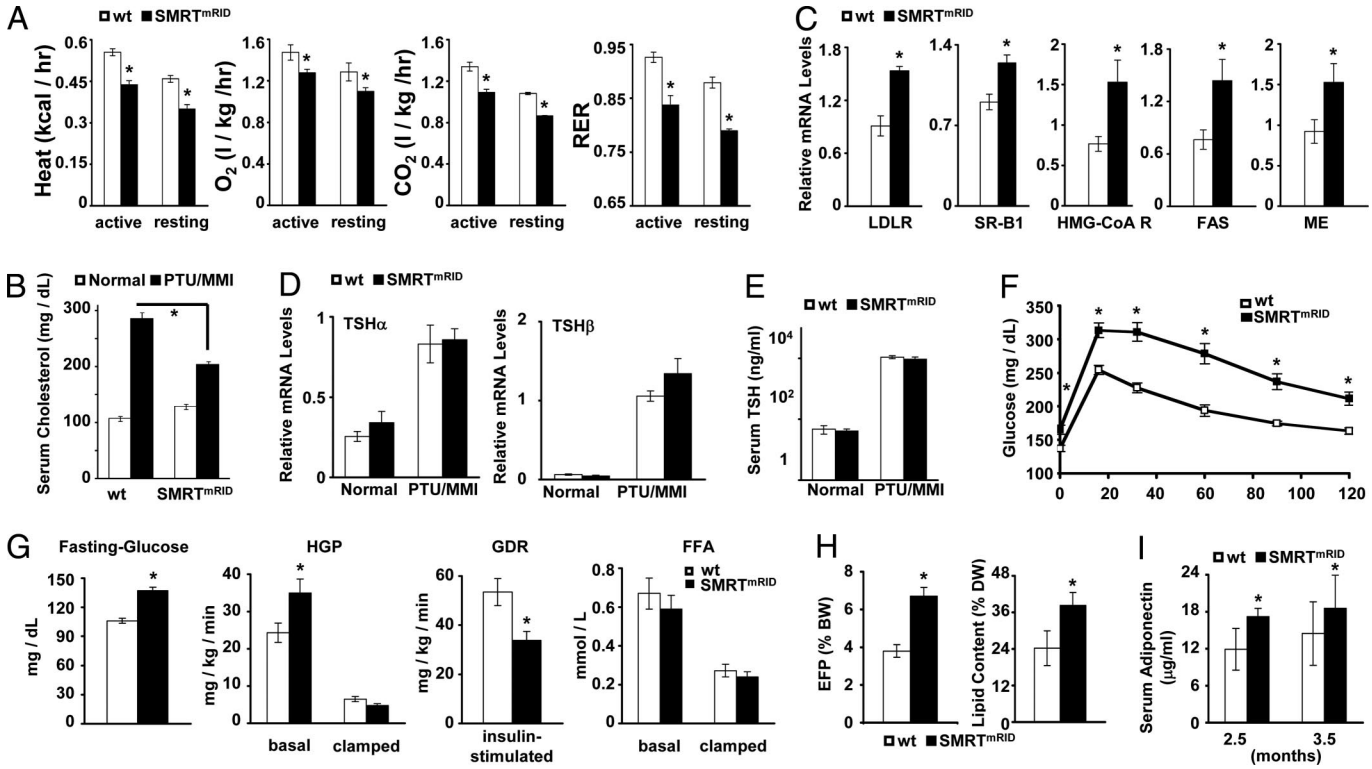

Fig. 2. SMRT^{mRID} mutant mice exhibit perturbed metabolic phenotype. (*A*) SMRT^{mRID} mice (10 weeks old, $n = 6$) display reduced heat production, O_2 consumption, CO_2 production, and respiratory exchange ratios (RERs). (*B*) Attenuated increase of serum cholesterol in SMRT^{mRID} mice [2–3 months old, $n = 7$ (wt) and 5 (SMRT^{mRID})] in PTU/MMI-induced hypothyroidism. (*C*) Derepression of TR target genes in PTU/MMI-treated SMRT^{mRID} livers. Pituitary TSHα and TSHβ mRNA expression (*D*) and serum TSH levels (*E*) are normal in untreated and PTU/MMI-treated conditions. (*F*) Glucose tolerance test revealed increased fasting blood glucose and intolerance to i.p. glucose injection in SMRT^{mRID} mice compared with controls (8 weeks old, $n = 12$). (*G*) Hyperinsulinemic-euglycemic clamping on chow-fed 4-month-old, weight-matched littermates ($n = 7$) revealed hepatic glucose production (HGP) was higher at baseline in SMRT^{mRID} animals, but suppressed to similar levels after insulin injection. Insulin-stimulated glucose disposal was significantly diminished. Free fatty acid levels were not changed. (*H*) Increased epididymal fat pad (EFP) to body weight ratio in SMRT^{mRID} as compared with WT ($n = 6$) on high-fat diet (HFD). Body composition analysis ($n = 10$) confirms an increased percentage of SMRT^{mRID} dry weight is composed of lipids. (*I*) Serum adiponectin levels are elevated in SMRT^{mRID} mice at 2.5 ($n = 13$) and 3.5 months ($n = 9$) of age. *, significant differences with *P* values <0.05 by using the student *t* test. Standard error of the mean (SEM) is shown unless otherwise indicated.

derived MEF lines and primary preadipocytes isolated from adult EFPs (data not shown). Interestingly, although wt-transformed MEFs require differentiation mixture to become adipocytes, ≈10% of SMRT^{mRID} cells display the unprecedented ability to spontaneously differentiate in the absence of any DC (Fig. 3*A*). Thus, in addition to changing adipogenic potential, SMRT-directed NR repression may act as the entry "checkpoint" of the adipocytic lineage.

Genome-Wide Gene Analysis Predicts PPARγ Pathway. The transcriptional profiles of SMRT^{mRID} and wt cell lines were compared at various time points before observable differences in cell morphology or lipid accumulation by using a genome-wide gene expression approach. At cell confluence, 2 days before the addition of DC, statistically significant changes were observed in the expression of ≈6,400 unique transcripts. Unbiased KEGG pathway analysis identified PPAR signaling as a major category among the differentially expressed genes, the vast majority of which were up-regulated in SMRT^{mRID} cells, including fatty acid binding protein 4 (Fabp4/aP2), the scavenger receptor CD36, and lipoprotein lipase (Lpl) (Table S1).

To confirm the microarray data and extend our analysis, we performed quantitative PCR on cells throughout the course of adipocyte differentiation (Fig. 3*B*). At day 0 (untreated), wt and SMRT^{mRID}-derived MEFs expressed comparably low levels of PPARγ. In the presence of DC for just 3 days, PPARγ was dramatically up-regulated in SMRT^{mRID} cells, with induction relative to wt cells exceeding 10-fold. Notably, basal expression of well-established PPARγ target genes including aP2, CD36, CEBPα, and LPL was enhanced in SMRT^{mRID} cells; these were more robustly induced and, in some cases, occurred earlier in the differentiation time course in SMRT^{mRID} relative to wt cells. We also observed enhanced basal and maximal expression levels of other lipid biosynthetic genes, including Scd1, Pcx1, and Dgat2 (Fig. 3*B*).

De-repression of PPARγ Enhances Adipogenic Capacity of SMRT^{mRID} Cells. To confirm that the SMRT mRID mutation indeed results in altered PPARγ signaling, we tested the SMRT^{mRID} and wt MEF lines for transactivation in response to cotransfection of a GAL4-PPARγ construct and an UAS-luciferase reporter and treatment with a synthetic PPARγ agonist, rosiglitazone (Rosi). The basal and ligand-stimulated transcriptional activity of PPARγ was enhanced in SMRT^{mRID} cells especially at low ligand concentrations (Fig. S4). This suggests that the SMRT^{mRID} mutation broadly affects PPARγ signaling by de-repressing basal activity, enhancing ligand sensitivity, and significantly increasing maximal transcriptional capacity.

Although PPARγ is widely accepted as the master regulator of adipogenesis, several other NHRs directly influence the process of adipogenesis (14–17). To verify the role of PPARγ in the enhanced adipogenesis observed in our SMRT^{mRID} MEFs, we stably expressed PPARγ shRNA in mutant and wt cells by lentiviral transduction and examined the influence of PPARγ knockdown on adipogenesis and gene expression. After 5 days of exposure to DC,

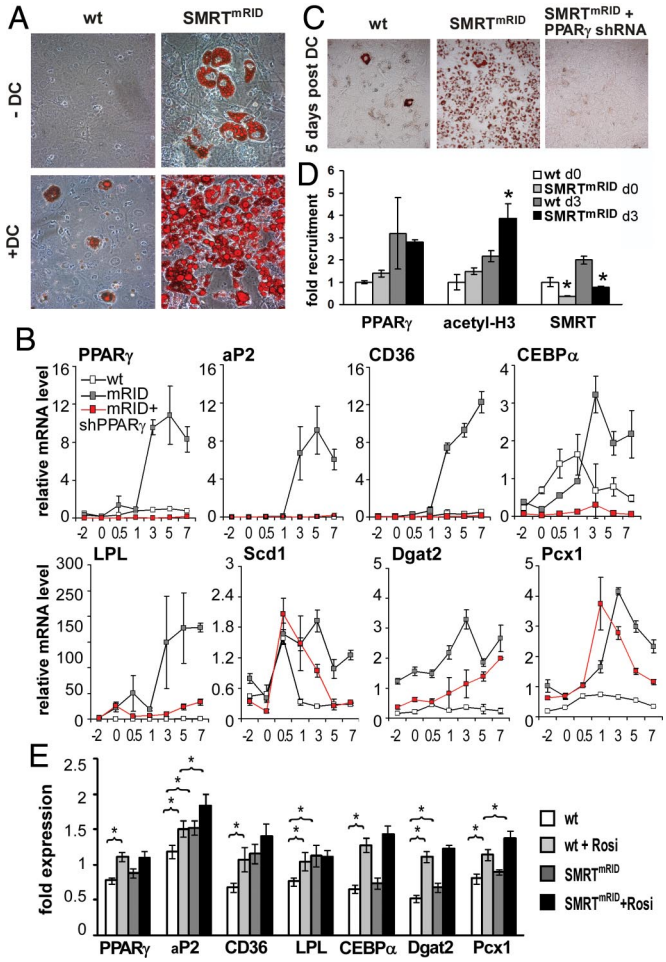

Fig. 3. SMRT^{mRID} MEFs exhibit enhanced adipogenic potential. (*A*) Postconfluent SMRT^{mRID}-derived MEFs after a 7-day exposure to DC. Oil Red O staining revealed nearly 100% differentiation of SMRT^{mRID} cells into mature adipocytes compared with wt (5%). Spontaneous adipocyte differentiation was seen in ≈10% of untreated SMRT^{mRID} cells. (*B*) Increased expression of PPARγ and PPARγ-target genes in SMRT^{mRID} MEFs during differentiation by using QPCR analysis. Expression levels under described experimental conditions are compared over time (indicated as days relative to addition of DC). (*C*) Lentiviral shRNA-knockdown of PPARγ expression abolished the adipogenic potential of SMRT^{mRID} MEFs as demonstrated by Oil Red O. (*D*) ChIP analysis of the aP2 promoter in the proximity of the PPRE revealed reduced SMRT occupancy and increased histone H3 acetylation. Immunoprecipitation was performed by using control IgG or antibodies against SMRT, PPARγ and acetyl-H3. (*E*) QPCR analysis of WAT from SMRT^{mRID} and wt mice that were treated with vehicle or Rosi for 5 days. Brackets with asterisks indicate $P < 0.05$.

≈5% of wt MEFs and nearly 100% of SMRT^{mRID} cells accumulated lipids indicative of adipocyte differentiation. Knockdown of PPARγ in these cells completely blocked adipocyte differentiation, suggesting that the enhanced adipogenesis observed in the SMRT^{mRID} is likely a PPARγ-dependent effect (Fig. 3*C*). To further explore the impact of the SMRT mutation on PPARγ in this system, we interrogated the expression of adipogenic PPARγ target genes over a time course of differentiation in SMRT^{mRID} cells with or without transduced shPPARγ. Indicative of the direct influence of the SMRT^{mRID} mutation on PPARγ regulation of target genes, aP2, CD36, and CEBPα were never induced above wt expression levels in SMRT^{mRID} MEFs stably expressing shPPARγ. LPL and Dgat2 expression were also dramatically reduced in the mutant cells in response to PPARγ knockdown (Fig. 3*B*). However, these genes are still expressed at levels significantly higher than in wt MEFs, likely reflecting multifactorial regulation of their expression. Collectively, these observations indicate that the enhanced adipogenic phenotype observed in SMRT^{mRID} cells is largely contributed by PPARγ de-repression.

Chromatin Immunoprecipitation. Chromatin immunoprecipitation (ChIP) was used to examine PPARγ binding, SMRT recruitment, and acetylation status of the aP2 promoter. As expected, promoter occupancy by SMRT was markedly reduced in SMRT^{mRID} cells compared with wt MEFs (Fig. 3*D*). Interestingly, PPARγ binding appears to be independent of SMRT association, maintaining relatively constant levels in both cell types. Additionally, significant increases in acetylated histone H3 were observed on the aP2 promoter of SMRT^{mRID} cells, suggesting that the rate at which PPARγ-associated coactivators are cycling is sufficiently increased to sustain enhanced acetylation along PPARγ-regulated promoters. It has been suggested that SMRT is not recruited to the aP2 promoter (18), however, it is important to note that our studies focus on preadipocytes where aP2 is Rosi responsive rather than mature adipocytes. Together with the genetic requirement for PPARγ, these results provide strong evidence that SMRT functions as a repressor of white adipose tissue (WAT) differentiation and that its association with PPARγ is essential for this effect.

In Vivo De-repression of PPARγ in SMRT^{mRID} Mice. To verify that PPARγ de-repression contributed to the increased insulin-sensitive adipose phenotype of SMRT^{mRID} mice in vivo, we examined gene expression in WAT from 8-week-old SMRT^{mRID} mice. Consistent with results from the transformed MEF lines, significant increases in the expression of aP2, Lpl, and Dgat2 were observed in SMRT^{mRID} WAT compared with controls (Fig. 3*E*). Treatment of these mice with 1 mg·kg^{-1}·day^{-1} Rosi for 7 days resulted in even greater induction of a collection of PPARγ targets in SMRT^{mRID} WAT relative to wt tissue. There was a trend toward enhanced induction of these genes, with the exception of Lpl, in the Rosi-treated mutant WAT, and both aP2 and Pcx1 were expressed at significantly higher levels in SMRT^{mRID} WAT than in similarly treated control samples. Interestingly, basal de-repression of aP2, CD36, and Lpl in SMRT^{mRID} WAT resulted in expression levels similar to those induced by ligand treatment in wt WAT (Fig. 3*E*). Collectively, these results support a model of enhanced adipocyte differentiation through reduced PPARγ repression, reprogramming "differentiation capacity" to 100% in vitro as well as increasing adiposity in vivo.

Discussion

Although it is clear that nuclear receptors play central roles in developmental, metabolic, and reproductive biology, the precise mechanisms by which they control these processes remain far less understood. The viability and normal organogenesis of the SMRT^{mRID} knockin mice described here demonstrate that the lethality of the SMRT knockout is due to non-NHR transcription factors. In contrast to the defects reported in the SMRT null cortex (10), the structural and cellular composition of the SMRT^{mRID} brain was normal. A slightly thinner ventricular wall was noted in the SMRT^{mRID} mice at birth, but this abnormality subsided by adulthood. Although a retinoid-associated vertebrate patterning defect is also observed (S.-H.H. and R.M.E., unpublished results), our collective data demonstrate that SMRT-dependent repression of NHR signaling is nonetheless expendable during development.

In contrast, the widespread metabolic changes observed in these mice provide the first direct evidence that SMRT-directed NHR repression is essential for normal metabolic homeostasis, regulating the TR and PPARγ pathways in vivo. The shift in differentiation capacity of SMRT^{mRID} MEFs in vitro from 5% to nearly 100% and the temporal compression suggests that SMRT-dependent NHR repression acts both to restrict lineage "capacity" and to moderate differentiation rate. Furthermore, because NCoR has been de-

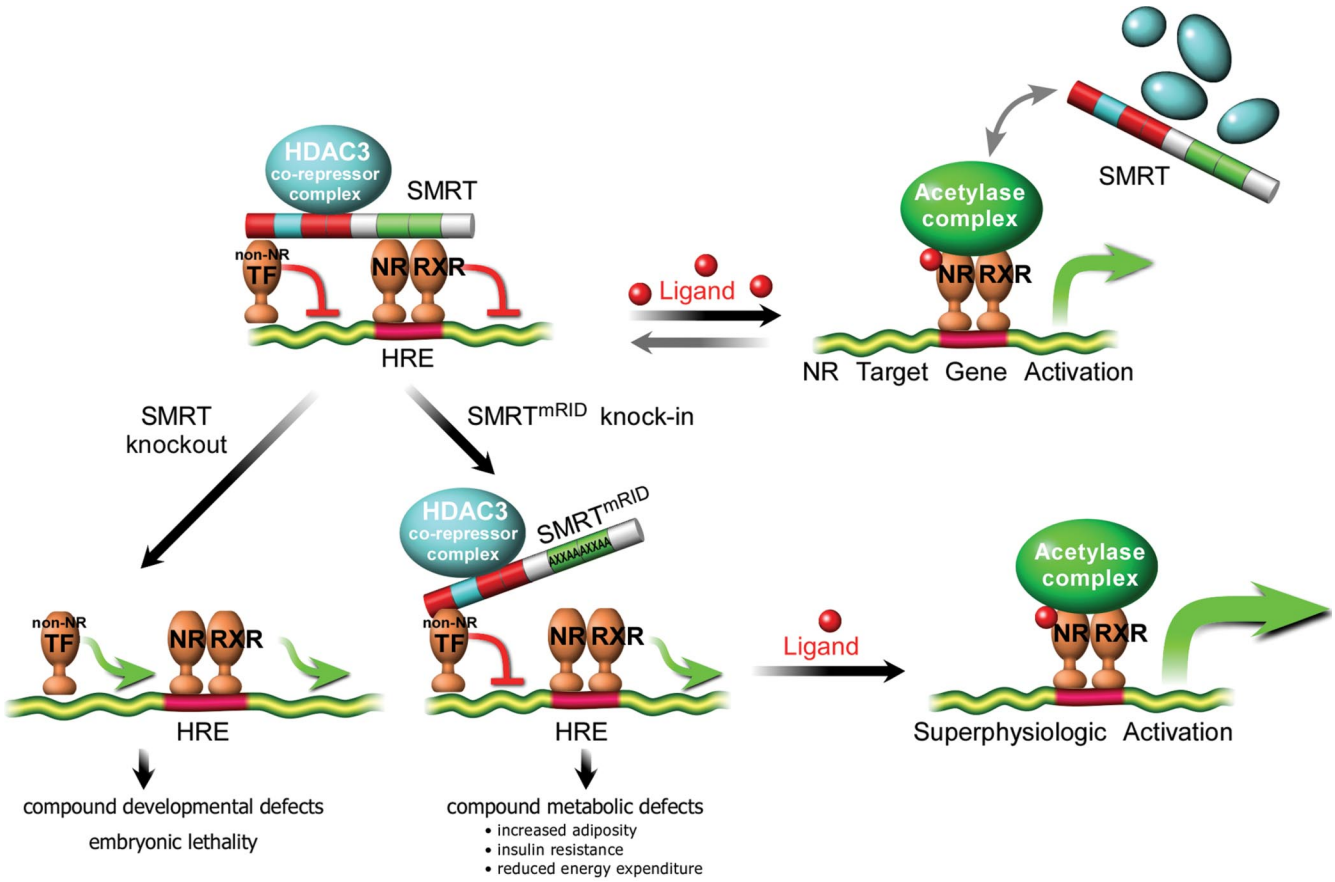

Fig. 4. Model for in vivo function of SMRT-mediated transcriptional repression. The corepressor SMRT is recruited by a wide variety of transcription factors, including NHRs, to mediate lineage- and signal-dependent transcriptional repression. In the standard model of NHR action, ligand binding is believed to actuate a bifunctional molecular switch, releasing the corepressor complex and recruiting a histone acetyltransferase coactivator complex, resulting in potent transcriptional activation of gene targets. Whole-body knockout of SMRT results in developmental defects and embryonic lethality. In contrast, mice with mutations that specifically disrupt SMRT interaction with NHRs are viable but display widespread metabolic defects, demonstrating that the lethality of SMRT knockout mice is mediated by non-NHR transcription factors. Derepression of SMRT enhances NHR sensitivity to ligand.

scribed to restrict progression down the astrocytic lineage in neural stem cells, the notion that corepressors may act through NHRs to influence lineage-specific differentiation may be a general phenomenon. Transcriptional regulation of differentiation rate has not previously been described. The loss of SMRT–NHR repression appears to dramatically increase the quantitative and temporal expression of adipogenic gene networks whose unbridled activity may overrun normal lineage checkpoints. This in vitro proadipogenic deregulation may directly translate to the observed increased in vivo adiposity as well as the compromised glucose/insulin response.

Physiology seeks to balance continually variable nutrient status against continually variable demand (Fig. 4 *Upper*). NR coactivators have been shown to contribute to the dynamics of this balance (3, 5); an example is RIP140, which is involved in energy metabolism in muscle, liver, and WAT (19–21). Investigation into the role of Sirt1 in nutrient metabolism has indicated that PPARγ repression may be at the crux of this balance and that SMRT may be directly involved in this process (22). Taking these studies into consideration, our data indicate that the set points of various metabolic processes are established by the dynamic recruitment of corepressors and coactivators to modulate chromatin and nuclear receptor signaling. Such a molecular balance would create a combinatorial mechanism with the capacity and complexity to modulate gene expression to meet physiologic demand.

These observations suggest that SMRT effectively acts as a genetic antagonist to TR and PPARγ ligand signaling. Thus, in $SMRT^{mRID}$ mutant mice and cells, the balance between repressive and active status is shifted to the right (Fig. 4 *Lower*), resulting in apparent increased potency of ligand as well as increased efficacy of the overall transcriptional response. The resultant cascade of proadipogenic changes apparently lowers the response threshold to dietary and endocrine cues, leading $SMRT^{mRID}$ mice toward increased adiposity and cell lines to enhanced adipogenesis. This mechanistic shift translates to an altered adipogenic set point and indicates that transcriptional repression is a key component of metabolic homeostasis by continuously limiting response to natural or synthetic ligands.

Materials and Methods

$SMRT^{mRID}$ Mice. Animals used in all experiments were age-matched males of comparable mixed genetic background (on average 50% sv129 and 50% C57BL/6). Mice were maintained in a temperature and light-controlled environment and received a standard diet (PMI laboratory rodent diet 5001, Harlan Teklad) unless otherwise noted.

Mammalian 2-Hybrid Analysis. CV-1 cells were cotransfected with VP-NHR LBD, Gal4 DBD-SMRT (wt or mRID), a UAS-luciferase reporter, and β-gal expression constructs by using Fugene HD (Roche) per manufacturer's instructions. Luciferase readings were normalized by β-gal activity to determine the influence of the mRID mutation on the affinity of SMRT for particular receptors.

Metabolic Studies. Real-time metabolic analyses were conducted in a Comprehensive Lab Animal Monitoring System (Columbus Instruments). These chambers are located in an undisturbed room under 12 h/12 h light/dark cycles. Experiments were repeated at least twice and chambers were alternated to avoid cage-specific

effects. For hypothyroid studies, 2- to 3-month-old wt and SMRT^{mRID} male mice were fed a low-iodine diet supplemented with 0.15% propylthiouracil (PTU) and 0.025% methimazole (MMI) in drinking water (Harlan Teklad) for 30 days ($n = 7$ and 5, respectively). Hypothyroidism was confirmed by determination of serum TSH levels measured as described in ref. 23. Serum cholesterol was measured in the same group of mice before and after PTU/MMI treatment. Total RNAs from pituitary glands and liver were used to generate cDNA for QPCR. A glucose tolerance test (GTT) was conducted after a 6-h fast. Mice were injected i.p. with 1.5 mg/g glucose and blood glucose was monitored at 30-min intervals by using OneTouch Ultra glucometer (Lifescan Inc). Body composition analysis was performed by desiccating eviscerated mice, followed by saponification in KOH and ethanol. Total volumes were measured and glycerol concentration was determined by calorimetric assay (Sigma).

Hyperinsulinemic-Euglycemic Clamp Studies. Three days after surgery, chronically cannulated mice were used to perform clamping studies as described in ref. 24. Basal blood glucose was measured 60 min before administration of glucose or insulin. At time 0, a primed constant infusion of 5 μCi/h, 0.12 ml/h of D-[3-^{3}H]glucose (NEN Life Science Products) was initiated, and a basal blood sample was drawn for determination of glucose-specific activity. After basal sampling, glucose (50% dextrose; Abbott) and insulin (12 mU·kg^{-1}·min^{-1}; Novo Nordisk) plus tracer (5.0 μCi/h) infusions were simultaneously initiated. Steady state was achieved when blood glucose was successfully clamped and the GIR fixed for a minimum of 30 min. At the end of the clamp, a blood sample was taken for the determination of glucose turnover.

Generation of SMRT^{mRID}-Derived MEF Lines. Embryonic fibroblasts were harvested from individual E15.5 mice. After confirming genotype, 2 independent cell lines were established from SMRT^{mRID} and wt littermates according to the 3T3 methodology established by Todaro and Green (25). Adipocyte differentiation was performed as described in ref. 16 by using DMI with 1 μM rosiglitazone.

Gene Expression Analysis. Total RNA was isolated from mouse tissue and cells by using TRIzol reagent (Invitrogen) according to the manufacturer's instructions. mRNA levels were quantified by QPCR with SYBR Green (Invitrogen). cDNA was synthesized from 1 μg of DNase-treated total RNA by using SuperScript II reverse transcriptase (Invitrogen). Samples were run in technical triplicates and relative mRNA levels were calculated by using the standard curve methodology and normalized against *36B4* mRNA levels in the same samples.

Affymetrix GeneChip Analysis. Undifferentiated SMRT^{mRID} and wt-derived MEFs were harvested and processed for RNA. Samples were labeled and hybridized to Affymetrix MG430 2.0 arrays according to the manufacturer's standard protocols. Analysis of the resulting profiles was carried out by using Vampire microarray software as described in ref. 26. Significance in this program was determined by using a Bonferroni value of 0.05.

Lentivirus Production and Generation of Stable Knockdown Cell Lines. Plasmids were constructed for the production of third-generation lentiviral vectors expressing shRNA against murine PPARγ by using human H1-RNA promoter. AD293 cells were cotransfected with lentiviral expression plasmids and packaging plasmids by using calcium phosphate. Lentivirus was harvested at 48 and 72 h after transfection and passed through 0.22-μm filters. Infection of SMRT^{mRID} and wt cell lines with PPARγ shRNA lentivirus was carried out by adding lentiviral supernatant to the cell culture and selecting for GFP expression by flow cytometry.

Chromatin Immunoprecipitation. SMRT^{mRID} or wt-derived MEFs were grown to confluence in DMEM supplemented with 10% FBS and subjected to a standard differentiation protocol. Approximately 2×10^8 cells were fixed with 1% formaldehyde followed by sonication to generate genomic DNA fragments ranging from 200 to 1,000 bp in length. After sonication, samples were blocked with protein A agarose beads preabsorbed with salmon sperm DNA (Upstate Biotechnology) at 4 °C for 1 h. Aliquots equal to 1/20 of the total volume were used as input controls. Immunoprecipitation was performed overnight at 4 °C by using control IgG or antibodies against SMRT (kindly provided by Dr. Jiemin Wong) (27), PPARγ (Santa Cruz), and acetyl-H3 (Upstate Biotechnology). Precipitated DNA was eluted with 1% SDS, 0.1% $NaHCO_3$ and NaCl was added to a final concentration of 0.3 M and heated at 65 °C to reverse the formaldehyde cross-linking. DNA fragments were phenol/chloroform extracted followed by ethanol precipitation. For qPCR, ap2 primers (5′-GAG CAA GGT CTT CAT CAT TAC G-3′, 5′-CCC CTG GAG CTG GAG TTA C-3′) were used to amplify genomic DNA precipitated by each antibody (23). Results were normalized by the amount of PCR products amplified from the corresponding input samples.

Accession Numbers. The GeneChip analysis data discussed in this publication have been deposited in National Center for Biotechnology Information's Gene Expression Omnibus under the GEO Series accession no. GSE13143 (http://www.ncbi.nlm.nih.gov/geo/query/acc.cgi?acc = GSE13143).

ACKNOWLEDGMENTS. We thank E. Banayo, H. Juguilon, J. Alvarez, and Y. Zou for technical assistance; J. Wong for anti-SMRT antibody; and E. Ong and S. Ganley for administrative assistance. R.R.N. was supported by Molecular Cardiology Training Grant T32 HL07770–14. J.W.J. is supported by a Human Frontier Science Program fellowship. C-H.L. is supported by the American Heart Association and American Diabetes Association and National Institutes of Health Grant R01DK075046. R.M.E. is an investigator of the Howard Hughes Medical Institute at the Salk Institute for Biological Studies and March of Dimes Chair in Molecular and Developmental Biology. This work was supported by the Howard Hughes Medical Institute and National Institutes of Health Grants 5R37DK057978 and 5R01HD027183.

1. Mangelsdorf DJ, *et al.* (1995) The nuclear receptor superfamily: The second decade. *Cell* 83(6):835–839.
2. Perissi V, Rosenfeld MG (2005) Controlling nuclear receptors: The circular logic of cofactor cycles. *Nat Rev Mol Cell Biol* 6(7):542–554.
3. Wang Z, *et al.* (2006) Critical roles of the p160 transcriptional coactivators p/CIP and SRC-1 in energy balance. *Cell Metab* 3(2):111–122.
4. Ge K, *et al.* (2002) Transcription coactivator TRAP220 is required for PPAR gamma 2-stimulated adipogenesis. *Nature* 417(6888):563–567.
5. Picard F, *et al.* (2002) SRC-1 and TIF2 control energy balance between white and brown adipose tissues. *Cell* 111(7):931–941.
6. Puigserver P, *et al.* (1998) A cold-inducible coactivator of nuclear receptors linked to adaptive thermogenesis. *Cell* 92(6):829–839.
7. Sonoda J, Mehl IR, Chong LW, Nofsinger RR, Evans RM (2007) PGC-1beta controls mitochondrial metabolism to modulate circadian activity, adaptive thermogenesis, and hepatic steatosis. *Proc Natl Acad Sci USA* 104(12):5223–5228.
8. Jepsen K Rosenfeld MG (2002) Biological roles and mechanistic actions of co-repressor complexes. *J Cell Sci* 115(Pt 4):689–698.
9. Jepsen K, Gleiberman AS, Shi C, Simon DI, Rosenfeld MG (2008) Cooperative regulation in development by SMRT and FOXP1. *Genes Dev* 22(6):740–745.
10. Jepsen K, *et al.* (2007) SMRT-mediated repression of an H3K27 demethylase in progression from neural stem cell to neuron. *Nature* 450(7168):415–419.
11. Hu X, Lazar MA (1999) The CoRNR motif controls the recruitment of corepressors by nuclear hormone receptors. *Nature* 402(6757):93–96.
12. Nagy L, *et al.* (1999) Mechanism of corepressor binding and release from nuclear hormone receptors. *Genes Dev* 13(24):3209–3216.
13. Perissi V, *et al.* (1999) Molecular determinants of nuclear receptor-corepressor interaction. *Genes Dev* 13(24):3198–3208.
14. Tontonoz P, Hu E, Spiegelman BM (1994) Stimulation of adipogenesis in fibroblasts by PPAR gamma 2, a lipid-activated transcription factor. *Cell* 79(7):1147–1156.
15. Hosono T, *et al.* (2005) RNA interference of PPARgamma using fiber-modified adenovirus vector efficiently suppresses preadipocyte-to-adipocyte differentiation in 3T3–L1 cells. *Gene* 348:157–165.
16. Fu M, *et al.* (2005) A nuclear receptor atlas: 3T3–L1 adipogenesis. *Mol Endocrinol* 19(10):2437–2450.
17. Gurnell M, *et al.* (2000) A dominant-negative peroxisome proliferator-activated receptor gamma (PPARgamma) mutant is a constitutive repressor and inhibits PPARgamma-mediated adipogenesis. *J Biol Chem* 275(8):5754–5759.
18. Guan HP, Ishizuka T, Chui PC, Lehrke M, Lazar MA (2005) Corepressors selectively control the transcriptional activity of PPARgamma in adipocytes. *Genes Dev* 19(4):453–461.
19. Seth A, *et al.* (2007) The transcriptional corepressor RIP140 regulates oxidative metabolism in skeletal muscle. *Cell Metab* 6(3):236–245.
20. Herzog B, *et al.* (2007) The nuclear receptor cofactor, receptor-interacting protein 140, is required for the regulation of hepatic lipid and glucose metabolism by liver X receptor. *Mol Endocrinol* 21(11):2687–2697.
21. Powelka AM, *et al.* (2006) Suppression of oxidative metabolism and mitochondrial biogenesis by the transcriptional corepressor RIP140 in mouse adipocytes. *J Clin Invest* 116(1):125–136.
22. Picard F, *et al.* (2004) Sirt1 promotes fat mobilization in white adipocytes by repressing PPAR-gamma. *Nature* 429(6993):771–776.
23. Pohlenz J, *et al.* (1999) Improved radioimmunoassay for measurement of mouse thyrotropin in serum: Strain differences in thyrotropin concentration and thyrotroph sensitivity to thyroid hormone. *Thyroid* 9(12):1265–1271.
24. Hevener AL, *et al.* (2003) Muscle-specific Pparg deletion causes insulin resistance. *Nat Med* 9(12):1491–1497.
25. Todaro GJ, Green H (1963) Quantitative studies of the growth of mouse embryo cells in culture and their development into established lines. *J Cell Biol* 17:299–313.
26. Hsiao A, Ideker T, Olefsky JM, Subramaniam S (2005) VAMPIRE microarray suite: A web-based platform for the interpretation of gene expression data. *Nucleic Acids Res* 33(Web Server issue):W627–W632.
27. Li J, Lin Q, Wang W, Wade P, Wong J (2002) Specific targeting and constitutive association of histone deacetylase complexes during transcriptional repression. *Genes Dev* 16(6):687–692.